

# Structural and dielectric properties of amorphous $\text{ZrO}_2$ and $\text{HfO}_2$

Davide Ceresoli\* and David Vanderbilt

*Department of Physics and Astronomy, Rutgers University,  
136 Frelinghuysen Road, Piscataway, New Jersey 08854, USA*

(Dated: June 13, 2006)

Zirconia ( $\text{ZrO}_2$ ) and hafnia ( $\text{HfO}_2$ ) are leading candidates for replacing  $\text{SiO}_2$  as the gate insulator in CMOS technology. Amorphous versions of these materials ( $a\text{-ZrO}_2$  and  $a\text{-HfO}_2$ ) can be grown as metastable phases on top of a silicon buffer; while they tend to recrystallize during subsequent annealing steps, they would otherwise be of considerable interest because of the promise they hold for improved uniformity and electrical passivity. In this work, we report our theoretical studies of  $a\text{-ZrO}_2$  and  $a\text{-HfO}_2$  by first-principles density-functional methods. We construct realistic amorphous models using the “activation-relaxation” technique (ART) of Barkema and Mousseau. The structural, vibrational, and dielectric properties of the resulting models are analyzed in detail. The overall average dielectric constant is computed and found to be comparable to that of the monoclinic phase.

PACS numbers: 77.22.-d, 61.43.Bn, 63.50.+x, 71.23.Cq

## I. INTRODUCTION

In recent years, a major thrust of applied development in the semiconductor industry has been the search for materials that could replace  $\text{SiO}_2$  as the gate dielectric in CMOS technology. Conventional scaling of  $\text{SiO}_2$  would require a gate-dielectric thickness shrinking below 1 nm in the near future, according to the International Technology Road Map for Semiconductors.<sup>1</sup> In this regime, conventional thermally-grown  $\text{SiO}_2$  is expected to fail because of issues of tunneling leakage current and reliability. There are therefore strong incentives to identify materials with dielectric constant  $\epsilon$  (or  $K$ ) much larger than that of  $\text{SiO}_2$  (at  $\epsilon=3.9$ ), as these could be grown as thicker films while still providing the needed capacitance.

Among the most promising materials are  $\text{ZrO}_2$  and  $\text{HfO}_2$ , which do have much higher dielectric constants and some other positive features as well (e.g., chemical stability). However, one of the great advantages of  $\text{SiO}_2$  has been the fact it forms an amorphous oxide ( $a\text{-SiO}_2$ ), thus allowing it to conform to the substrate with enough freedom to eliminate most electrical defects at the interface. On the other hand,  $\text{ZrO}_2$  and  $\text{HfO}_2$  (which are very similar in many of their physical and chemical properties) are refractory materials, their melting temperature being 2988 K and 3085 K respectively. They are not good glass-formers;  $a\text{-ZrO}_2$ , for example, has been shown to recrystallize during growth if the growth temperature is too high (with tetragonal and monoclinic phases starting to appear above  $\sim 500^\circ\text{C}$  and  $\sim 700^\circ\text{C}$  respectively).<sup>2</sup> Thus, while  $\text{ZrO}_2$  and  $\text{HfO}_2$  can be grown as metastable amorphous phases on Si using low-temperature deposition techniques, films of this type unfortunately tend to recrystallize during the subsequent annealing steps that are required in current industrial fabrication processes.

Nevertheless, it is possible that admixing (alloying) with Si, Al, N, or other chemical constituents, or other strategies yet to be identified, may help to mitigate the recrystallization problem and stabilize the amorphous

phase.<sup>2</sup> In any case, it may be advantageous to study amorphous structures as a first step in understanding why the recrystallization is facilitated. With these motivations, we have embarked on a theoretical study of the structural and dielectric properties of amorphous zirconia and hafnia ( $a\text{-ZrO}_2$  and  $a\text{-HfO}_2$ ). In earlier work,<sup>3</sup> we generated models of  $a\text{-ZrO}_2$  using an *ab-initio* molecular dynamics approach in a plane-wave pseudopotential framework, and studied their structural and dielectric properties. In a subsequent publication,<sup>4</sup> we described an alternate and more efficient method of generating amorphous structures based on the activation-relaxation technique (ART) of Barkema and Mousseau,<sup>5</sup> and presented a few preliminary results on amorphous  $\text{ZrO}_2$  obtained using this approach. These calculations were carried out using a local-orbital basis approach embodied in the SIESTA code package.<sup>6</sup> In the present work, we systematically use SIESTA for all of the reported calculations. We first briefly review our implementation of the ART approach, and then embark on a systematic description of the generated  $a\text{-ZrO}_2$  and  $a\text{-HfO}_2$  structures and a comparison of their computed electronic, structural, and dielectric properties.

The paper is organized as follows. In Secs. II and III we describe the details of our electronic-structure calculations and of our procedure for generating amorphous models, respectively. We then describe the results of our calculations for  $\text{ZrO}_2$  in Sec. IV and for  $\text{HfO}_2$  in Sec. V. We also present some results concerning the Born dynamical effective charges and the dielectric activity for both systems in Sec. VI. We then finish with a conclusion in Sec. VII.

## II. COMPUTATIONAL DETAILS

We performed *ab-initio* density-functional theory (DFT) calculations<sup>7</sup> in the local-density approximation (LDA)<sup>8</sup> using a local-orbital expansion of the Bloch wave-

function as implemented in the SIESTA code.<sup>6</sup> The use of localized-orbital basis allows the retention of good accuracy in the DFT calculations at a reduced computational cost relative to plane-wave codes. A cutoff of 150 Ry was used for the expansion of the charge density, and all calculations were performed using  $\Gamma$ -point Brillouin zone sampling only. The dynamical matrix and Born effective charges were computed using the SIESTA via a finite-difference approach in which each atom was displaced by  $\pm 0.05 \text{ \AA}$  in the three cartesian directions and the forces and polarization changes were computed.

Two kind of basis sets were employed in the calculations. A minimal single- $\zeta$  basis set was used for the amorphization procedure, which required a large number of structural relaxations, while a larger triple- $\zeta$  basis set was used for the structural relaxation of the final structure and for the calculation of the lattice dielectric constant and of the infrared activity. Such a two-stage procedure (amorphization with a lower-level theory followed by annealing and relaxation with a higher-level theory) is a natural way of establishing a trade off between computational cost and accuracy; it has many precedents in the literature, as for example the generation of an amorphous structure by the use of empirical potentials followed by a first-principle annealing run in the work of Sarnthein *et al.*<sup>9</sup>

Because we were concerned that the minimal basis might not accurately reproduce the delicate interplay between ionic and covalent bonding in  $\text{ZrO}_2$  and  $\text{HfO}_2$ , the parameters for the minimal basis set were optimized following the prescription of Ref. 10 in order to ensure the correct energy ordering of the cubic, orthorhombic and monoclinic phases of  $\text{ZrO}_2$  and  $\text{HfO}_2$ . We then obtain  $E_{\text{cub}} - E_{\text{tet}} = 62 \text{ meV}$  and  $E_{\text{tet}} - E_{\text{mono}} = 89 \text{ meV}$  for  $\text{ZrO}_2$ , to be compared with values of 44 meV and 45 meV, respectively, computed using plane-wave methods and reported in Ref. 11. Here  $E_{\text{cub}}$ ,  $E_{\text{tet}}$ , and  $E_{\text{mono}}$  are the energies per formula unit of the cubic, tetragonal, and monoclinic phases, respectively of  $\text{ZrO}_2$ . Similar results are found for  $\text{HfO}_2$ . The relaxed structural parameters are also found to agree well. Thus, despite their simplicity, our optimized minimal basis sets for  $\text{ZrO}_2$  and  $\text{HfO}_2$  are able to capture the essentials of the structural energetics of the three crystalline phases.

### III. AMORPHIZATION PROCEDURE

In a previous study,<sup>3</sup> we carried out *ab-initio* molecular dynamics (MD) simulations of a 96-atom supercell in a melt-and-quench fashion in order to generate a structural model for  $\alpha$ - $\text{ZrO}_2$ . Because of the short time interval accessible to simulations, the cooling rate ( $3.4 \times 10^{14} \text{ K/s}$ ) was far beyond the fastest cooling rate that can be obtained experimentally by pulsed laser techniques. The fast cooling rate does not allow long-time-scale relaxation of system, which might be important in the case of relatively poor glass formers such as  $\text{ZrO}_2$  and  $\text{HfO}_2$ .

In order to see if the fast cooling rate could bias the resulting amorphous structure, we generated an independent amorphous sample<sup>4</sup> by using the ART event-based structural-evolution approach.<sup>5</sup> An event-based method leads to an accelerated dynamics and to a better sampling of long-time-scale modes in glasses. Rather than following the irrelevant details of the atomic motions as atoms vibrate back and forth about their average positions for long periods between activated events, ART focuses on simulating jumps over the barriers that separate the different basins of attraction of different local minima in the energy landscape. Thus, it requires a given computational effort per activated hop instead of per vibrational period. For disordered systems, which tend to show slow evolution, these two time scales may differ by many orders of magnitude, and this event-based technique therefore allows a much faster simulation.

We implemented the ART method as a driver for the *ab-initio* code SIESTA.<sup>6</sup> The flowchart of our implementation of the ART method can be found in Ref. 4. As reported there, we found that, starting from a 96-atom supercell made from the perfect cubic fluorite crystal structure, a number of Monte-Carlo (MC) trials equal to 5 times the number of atoms (i.e.,  $\sim 500$ ) was sufficient to produce a good amorphous structure. In our case, a MC temperature of 3000 K produced an acceptance ratio of 13%. Moreover, we found that during the first 50 MC trials, the acceptance ratio was higher ( $\sim 40\%$ ) and dropped down in the subsequent trials. We did not attempt to perform longer simulations at a lower MC temperature in order to “anneal” the system further.

### IV. RESULTS FOR $\text{ZrO}_2$

An important issue is the density of the amorphous phase, which, to our knowledge, is not accurately known experimentally. This issue was explored in our previous papers<sup>3,4</sup> and we found that among the initial guesses, a density between  $4.86 \text{ g/cm}^3$  and  $5.32 \text{ g/cm}^3$  generates a robust amorphous structure for  $\text{ZrO}_2$ .<sup>12</sup>

The ART simulation was performed at a constant volume corresponding to a density of  $5.32 \text{ g/cm}^3$ . A snapshot of the system is essentially indistinguishable, at the visual level, from that of the melt-and-quench MD-generated system of Ref. 3. The corresponding distribution of coordination numbers is shown in Fig. 1. We find a prevalence of 7- and 6-coordinated Zr over 8-coordinated Zr and a prevalence of 3- and 4-coordinated oxygens, similar to what was found for the MD-generated structure. (For comparison, recall that the monoclinic structure has 7-fold cations and equal numbers of 3- and 4-fold anions.)

One may wonder if such a spread of coordination numbers is actually due to intrinsic coordination defects such as dangling bonds or non-bridging oxygens (which are often present in other oxides such as  $\text{SiO}_2$ ). We monitored the electronic density of states at every MC accepted move and we found that occasionally a defective struc-

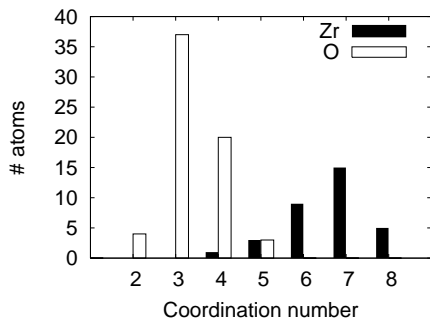


FIG. 1: *a*-ZrO<sub>2</sub> distribution of coordination numbers resulting from the activation-relaxation (ART) simulation. Zr and O atoms are indicated by filled and open bars, respectively.

ture (i.e., with some levels in the gap) is accepted. We also found, however, that the coordination defects are promptly saturated in subsequent MC moves. The final amorphous sample is a good insulator with an electronic gap of  $\sim 3.4$  eV.

Furthermore, the calculated phonon spectrum, shown in Fig. 2, is found to extend over approximately the same range of frequencies ( $50$ - $800$   $\text{cm}^{-1}$ ) and to show features similar to those of the sample obtained by the melt-and-quench MD simulation. The computed Born effective charges are slightly larger on average,  $Z^*(\text{Zr})=+5.08$  and  $Z^*(\text{O})=-2.54$ . Our lattice dielectric tensor is

$$\epsilon_{\text{latt}} = \begin{pmatrix} 17.9 & -0.7 & 0.2 \\ -0.7 & 17.5 & -0.5 \\ 0.2 & -0.5 & 14.1 \end{pmatrix} \quad (1)$$

yielding an average dielectric constant of 16.5, compared to the value of 17.6 of the MD-generated model, due to the fact that the vibrational spectrum is shifted to slightly higher frequencies. Assuming a value of  $\epsilon_{\infty} = 4.6$

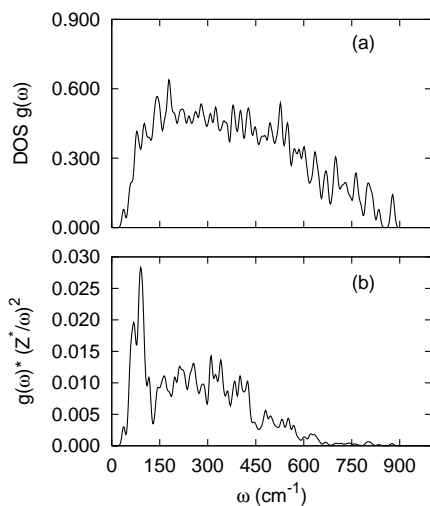


FIG. 2: (a) *a*-ZrO<sub>2</sub> phonon density of states (DOS) vs frequency. (b) *a*-ZrO<sub>2</sub> infrared activity (phonon DOS weighted by  $\tilde{Z}_{\lambda}^2/\omega_{\lambda}^2$ ) vs frequency.

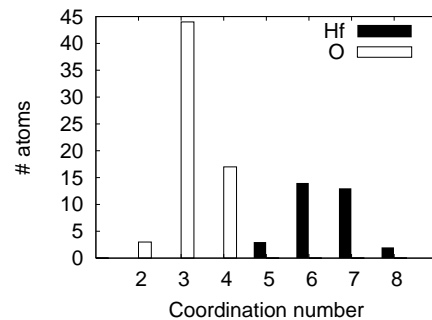


FIG. 3: *a*-HfO<sub>2</sub> distribution of coordination numbers resulting from the activation-relaxation (ART) simulation. Hf and O atoms are indicated by filled and open bars, respectively.

for the high-frequency dielectric constant,<sup>3</sup> the static dielectric constant yields a value of  $\sim 21$ , in good agreement with experimental values<sup>13</sup> and with the previous calculation.<sup>3</sup>

## V. RESULTS FOR HfO<sub>2</sub>

The amorphization of HfO<sub>2</sub> was carried out in a manner very similar to that used for its twin oxide ZrO<sub>2</sub>. For HfO<sub>2</sub>, however, we avoided the tedious procedure of performing independent melt-and-quench simulations in order to find a suitable density that can sustain an amorphous structure. Instead, we started the ART simulation at the same volume as for ZrO<sub>2</sub>,  $38.45 \text{ \AA}^3$  per unit formula (corresponding to an HfO<sub>2</sub> mass density of  $9.09 \text{ g/cm}^3$ ). Then, every 10 accepted MC moves, we performed a relaxation of the supercell volume. The final amorphous HfO<sub>2</sub> sample had a density of  $9.39 \text{ g/cm}^3$  (corresponding to  $37.22 \text{ \AA}^3$  per unit formula, 3.2% smaller than that of

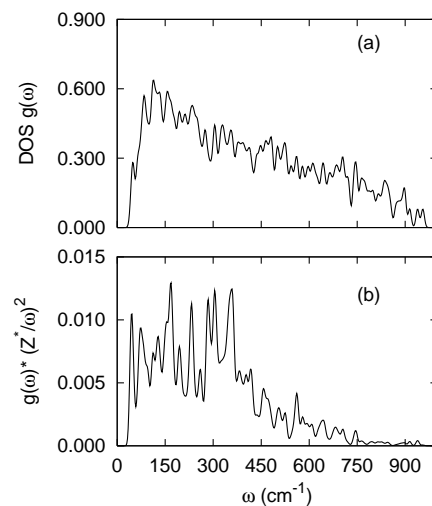


FIG. 4: (a) *a*-HfO<sub>2</sub> phonon density of states (DOS) vs frequency. (b) *a*-HfO<sub>2</sub> infrared activity (phonon DOS weighted by  $\tilde{Z}_{\lambda}^2/\omega_{\lambda}^2$ ) vs frequency.

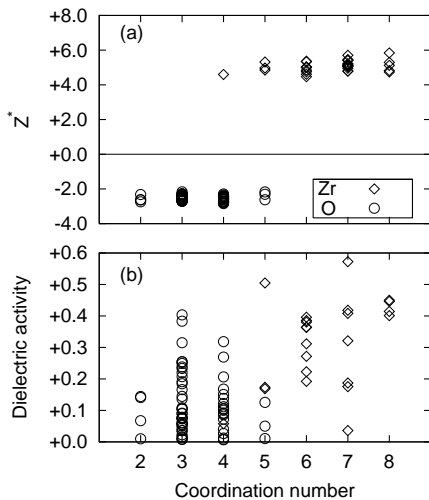


FIG. 5: (a) Scatter plot of isotropically averaged atomic  $Z^*$  values (vertical axis) vs atom type and coordination number (horizontal axis) for  $a$ - $ZrO_2$ . Circles and diamonds denote O and Zr atoms, respectively. (b) Same but with “dielectric activity” (see Eq. (5) of Ref. 3) plotted vertically.

$ZrO_2$ ). Experimentally, the unit cell volumes of the monoclinic and cubic phases are  $\sim 2\%$  larger in  $HfO_2$  than in the corresponding  $ZrO_2$  phases.<sup>11</sup>

The distribution of coordination numbers of the resulting  $a$ - $HfO_2$  sample is shown in Fig. 3. The average coordination number shows a prevalence of 7- and 6-coordinated Hf over 8-coordinated Hf, and a prevalence of 3- and 4-coordinated oxygens, as in the monoclinic structure. Compared to  $a$ - $ZrO_2$  (Fig. 1) there is a slightly higher prevalence of 3-coordinated oxygens, while the distribution of 6- and 7-coordinates cations is broadly similar. However, it is doubtful whether the small differences between  $ZrO_2$  and  $HfO_2$  that are visible in Figs. 1 and 3 are statistically significant.

The generated  $a$ - $HfO_2$  sample is found to be insulating, with a gap of  $\sim 3.8$  eV. Its calculated phonon spectrum, shown in Fig. 4, extends over approximately the same range of frequencies ( $50$ - $800$   $cm^{-1}$ ) as for  $a$ - $ZrO_2$ . Compared to Fig. 2(b), the infrared activity for  $HfO_2$  in Fig. 4(b) shows a broader feature in the  $50$ - $400$   $cm^{-1}$  frequency range. The computed Born effective charges are found to be smaller, on average, compared to those of  $a$ - $ZrO_2$ :  $Z^*(Hf)=+4.8$  and  $Z^*(O)=-2.4$ . Our computed lattice dielectric tensor

$$\epsilon_{\text{latt}} = \begin{pmatrix} 23.4 & -5.1 & -1.2 \\ -5.1 & 14.4 & 0.2 \\ -1.2 & 0.2 & 12.6 \end{pmatrix} \quad (2)$$

yields an average lattice dielectric constant of 16.8. Assuming a value of  $\sim 5$  for the high-frequency dielectric constant ( $\epsilon_\infty$ ),<sup>11</sup> the static dielectric constant yields a value of  $\sim 22$ , confirming again the striking similarity between  $a$ - $ZrO_2$  and  $a$ - $HfO_2$ .

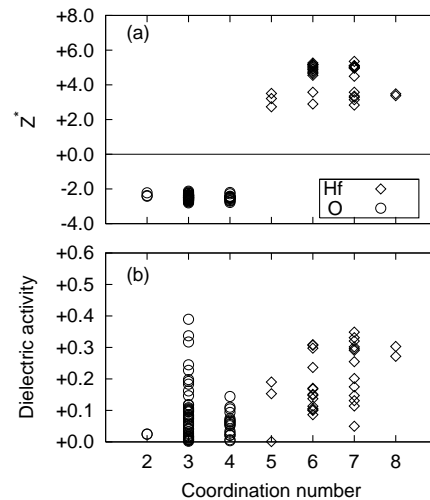


FIG. 6: (a) Scatter plot of isotropically averaged atomic  $Z^*$  values (vertical axis) vs atom type and coordination number (horizontal axis) for  $a$ - $HfO_2$ . Circles and diamonds denote O and Hf atoms, respectively. (b) Same but with “dielectric activity” (see Eq. (5) of Ref. 3) plotted vertically.

## VI. BORN CHARGES AND DIELECTRIC ACTIVITY

Clearly it is desirable to understand more fully the various contributions to the lattice dielectric response of the amorphous forms of  $ZrO_2$  and  $HfO_2$ . To this end, we decomposed various lattice properties by “atom type” (that is, by chemical species and coordination number) in the hope that such an analysis may provide further insight into our numerical results. This type of analysis was explained in detail and applied to the  $a$ - $ZrO_2$  sample generated using the MD melt-and-quench approach in Ref. 3.

Our results for the ART-generated samples are presented in Figs. 5 and Fig. 6. In the top panel of each figure, we report the Born effective charges as a function of the chemical species and coordination number. In both cases, the Born effective charges tend to be surprisingly independent of coordination number, and quite similar to the values found in the crystalline phases.<sup>11</sup> However, a mild tendency of the effective charge to increase with increasing coordination number of the cation is visible especially for Zr; it is also present for Hf but is partially obscured by larger fluctuations of the effective charges in that case.

The atom-resolved dielectric activity, defined in Eq. (5) of Ref. 3, is presented in Figs. 5(b) and 6(b). This is essentially a measure of the contribution of each type of atom to the lattice dielectric constant. Some trends are visible, such as a stronger contribution by 3-fold than by 4-fold oxygens, and a tendency to have larger contributions from higher-coordinated cations. However, even within any one atom type, there is a surprising degree of variation, with some atoms contributing strongly and

others contributing very little. Since the effective charges do not have nearly such a large variation, we infer that the differences must arise because of differences in the force-constant matrix elements. That is, some atoms may be regarded as being strongly anchored in place so that they contribute only weakly to the dielectric activity, while others participate in one or more soft modes and contribute strongly.

## VII. CONCLUSIONS

In conclusion, we have applied *ab-initio* electronic structure methods to study the lattice dynamics and dielectric properties of amorphous high- $K$  materials  $\alpha$ -ZrO<sub>2</sub> and  $\alpha$ -HfO<sub>2</sub>. We used the ART event-based technique to generate structural models of these amorphous materials. These 96-atom supercell models display a distribution of coordination numbers (mostly 3- and 4-fold for oxygen and 6-, 7- and 8-fold for Zr and Hf) but nonetheless remain insulating with a robust gap. The full force-constant matrix was computed for each supercell model, and the phonon density of states was calculated. In addition, the full Born-charge tensors were also computed for each model, and when combined with the force-constant information, the lattice dielectric response was obtained. The total dielectric constant is computed to be  $\sim 22$  for both materials, comparable to that of the monoclinic phase. Finally, the Born charges and the contributions to the dielectric activity were further analyzed by atom type. The effective charges are relatively uniform and are roughly similar to those of the crystalline

phases, whereas there are strong variations in the individual atomic contributions to the dielectric activity resulting from variations in soft-mode participation.

Several caveats are in order. First, while our ART procedure can be regarded as corresponding to a slower quench than in the previous MD-based calculations,<sup>3</sup> it is still very fast relative to any experimental quenching time scale, so that our models might have more defects than the experimental systems of interest. Second, real amorphous systems are generally grown at sufficiently low temperature to avoid crystallization, and not quenched from a melt. Thus, there could be significant differences in the resulting structures (for example, a greater tendency to void formation in the experimental samples). Third, our samples are perfectly stoichiometric and impurity-free, which will not generally be true of experimental samples. Finally, while a statistical analysis of an ensemble of ART-generated samples would be very desirable, the computational burden needed to carry out the above analysis for even a single sample is quite demanding. Nevertheless, we believe that the present results reveal the broad qualitative features to be expected for these amorphous phases, and constitute an important step forward on the road to a better understanding of these important materials.

## Acknowledgments

D.C. acknowledges J. Junquera for useful discussions and advice on basis set optimization. This work was supported by NSF Grant DMR-0233925.

---

\* Present address: Scuola Internazionale Superiore di Studi Avanzati (SISSA) and DEMOCRITOS, via Beirut 2-4, I-34014 Trieste, Italy

<sup>1</sup> International Technology Road-map for Semiconductors, 2001 Ed. <http://public.itrs.net/>.

<sup>2</sup> J. Zhu and Z.G. Liu, Appl. Phys. A—Materials Science and Processing **78**, 741 (2004).

<sup>3</sup> X. Zhao, D. Ceresoli, and D. Vanderbilt, Phys. Rev. B **71**, 085107 (2005).

<sup>4</sup> D. Vanderbilt, X. Zhao and D. Ceresoli, Thin Solid Films **486**, 125 (2005).

<sup>5</sup> G.T. Barkema and N. Mousseau, Phys. Rev. Lett. **77**, 4358 (1996); N. Mousseau and G.T. Barkema, Phys. Rev. B **61**, 1898 (2000).

<sup>6</sup> J.M. Soler, E. Artacho, J.D. Gale, A. García, J. Junquera, P. Ordejón, and D. Sánchez-Portal, J. Phys. Cond. Matter **14**, 2745 (2002).

<sup>7</sup> P. Hohenberg and W. Kohn, Phys. Rev. **136**, 864 (1964); W. Kohn and J.L. Sham, Phys. Rev. **140**, 1133 (1965).

<sup>8</sup> D.M. Ceperley and B.J. Alder, Phys. Rev. Lett. **45**, 566 (1980).

<sup>9</sup> J. Sarnthein, A. Pasquarello and R. Car, Phys. Rev. Lett. **74**, 4682 (1995); A. Pasquarello and R. Car, Phys. Rev. Lett. **79**, 1766 (1997).

<sup>10</sup> E. Anglada, J.M. Soler, J. Junquera and E. Artacho, Phys. Rev. B **66**, 205101 (2002).

<sup>11</sup> X. Zhao and D. Vanderbilt, Phys. Rev. B. **65**, 075105 (2002); X. Zhao and D. Vanderbilt, Phys. Rev. B. **65**, 233106 (2002).

<sup>12</sup> This density corresponds to the “7-cell” in Table III of Ref. 3.

<sup>13</sup> L. Koltunski and R.A.B. Devine, Appl. Phys. Lett. **79**, 320 (2001).